JJMIE

Volume 20, Number 3, September 2026
ISSN 1995-6665
Pages 361– 371
https://doi.org/10.59038/jjmie/200304
Editor-in-Chief: Prof. Faris M. AL-Oqla

Jordan Journal of Mechanical and Industrial Engineering

Enhanced Tribological and Thermal Performance of Gray Cast Iron via Electroless Ni–P Coating: Microstructural, Mechanical, and Electrochemical Insights

Moqdad J. Dakhil[1], Nabaa Sattar Radhi[1], Zainab Al-Khafaji[2,3*]

[1] *Department of Metallurgical, College of Materials Engineering, University of Babylon, Babylon, Iraq.*
[2] *Department of Civil Engineering, Faculty of Engineering and Built Environment, Universiti Kebangsaan Malaysia, 43600 UKM Bangi, Selangor, Malaysia.*
[3] *Imam Ja'afar Al-Sadiq University; Qahira, Baghdad, Iraq.*

Received 10 Aug 2025 *Accepted 20 Apr 2026*

Abstract

Gray cast iron (GCI) is widely used in automotive and industrial applications due to its good castability and cost efficiency; it is, however, limited by inferior wear resistance, high frictional losses, and susceptibility to corrosion when under severe service conditions. A detailed study was undertaken to improve the functional performance of GCI by plating a high-phosphorus electroless nickel–phosphorus (Ni–P) layer. An even Ni–P film of 12 wt. % phosphorus was chemically deposited using an autocatalytic electroless method followed by a heat treatment at 400 °C to induce partial crystallization. The microstructure and phase evolution of coatings were systematically characterized by SEM, EDS mapping and XRD; it was demonstrated that the coating was a mainly amorphous matrix consisting of nanocrystalline Ni_3P precipitates. Surface hardness of the coated surface was found to increased significantly from 290 HV of uncoated sample to a maximum value of 961 HV, which is corresponding to an improvement by a factor of about 231%. The thermal expansion analysis showed improved dimensional stability with a CTE value which was reduced from 0.25×10^{-6} to 0.19×10^{-6} °C^{-1}. Electrochemical performance was performed by potentiodynamic polarization and electrochemical impedance spectroscopy (EIS) in 3.5 wt. % NaCl solution. The corrosion potential for the Ni–P coating was positively shifted, with higher polarization resistance and decreasing impedance response since pulsing compared to GCI directly, which demonstrates better barrier protection and charge transfer kinetics are prohibited. Tribological evaluation in dry sliding also revealed a significant drop in friction coefficient, from around 0.65 to 0.07–0.10, as well as mild wear and intact state of the coating.

Keywords: Cast Iron, Nickel-phosphorus coating, Thermal Expansion,Pin on disc, coefficient of friction (COF).

1. Introduction

Gray cast iron (GCI) is still one of the most used among the available cast material, especially in engineering and industrial sectors owing to its outstanding castability properties, low cost, vibration damping capabilities, and moderate mechanical properties. It finds extensive applications in automotive, marine and heavy duty components such as engine blocks, brake rotors, rolling mill rolls, pump housings [1–3]. But the intrinsic disadvantages of GCI, such as bad wear resistance, corrosion easily and high friction losses greatly restrict its long-term working ability under harsh mechanical and thermal operations [4]. For instance, frictional contact at piston–cylinder interfaces in internal combustion (IC) engines contributes to 20–40% of the mechanical energy wasted [5,6] causing not just efficiencies but also materials deterioration due to it. With increasing use of biodiesel recently, corrosion wear of engine parts has become more serious, because the oxidative instability and high acid value is greater in these fuels, therefore it is urgent to develop surface engineering approach to address this issue[7].

Surface modification by electroless Ni–P (nickel-phosphorus) coating is attractive for enhancing the surface durability of metallic substrates while maintaining the bulk properties[8–12]. As a result of these advantages, the electroless deposition has become a versatile technique as it allows uniform thickness, low cost and coating on complex geometry without any need for external electric power [13,14]. It is interesting to note that the higher phosphorus Ni-P coatings (10-14) wt. % P are usually amorphous and have superior hardness, corrosion resistance, low frictional characteristics [15]. When subjected to heat treatment, the amorphous matrix is in part transformed into intermetallic phases such as Ni_3P and Ni_2P, resulting in improved hardness and tribological properties [16,17].

* Corresponding author e-mail: p123005@siswa.ukm.edu.my.

Recent investigations have reported the improvement of tribological and corrosion properties in steels and light alloys utilizing electroless Ni–P coatings [18–20]. For instance, Dhakal et al. [21]demonstrated improved wear resistance of Ni–P coated substrates under elevated temperatures, while Li et al. [22] highlighted the resistance against corrosion of amorphous Ni–P layers in saline environments. However, the literature lacks an integrated and systematic evaluation of the combined tribological, thermal, and electrochemical behavior of Ni–P coatings applied specifically to gray cast iron substrates[23]. Furthermore, most previous studies did not quantitatively correlate microstructural evolution (e.g., phase transformation and coating morphology) with functional performance under varying loading and thermal conditions.

Many reports have compared electroless Ni–P coatings with some of these traditional industrial surface engineering technologies. Electroless Ni–P coatings have been shown to achieve hardnesses similar to that of traditional hard chromium coatings along with competitive corrosion resistance, together with the additional benefit of eliminating the environmental and health hazards associated with hexavalent chromium processes [24]. Review articles on advanced tribological coatings also recognize electroless deposition as a mature and versatile surface modification process, along with physical vapor deposition (PVD) and thermal spray processes with their unique advantages and disadvantages in wear resistance, corrosion protection, coating thickness uniformity, and capability to coat complex geometries [25]. Comparative tribological studies have also indicated that electroless Ni–P films can act as an excellent interlayer or undercoat to improve the adhesion, load bearing capacity and overall tribological behaviour of hard PVD coatings like CrN and CrAlN, especially upon soft substrates [26]. However, it has been reported that some advanced or multi-layer coating systems potentially can surpass electroless Ni–P with respect to hardness and corrosion resistance if compositional designing or post-annealing is well optimized, thus highlighting the significance of application-tailored coatings [27].

The main objective of this work was to investigate, in an integrated way, the effects of a high phosphorus electroless nickel–phosphorus (Ni–P) coating on improving mechanical, thermal, tribological as well as electrochemical behavior gray cast iron. The research is concentrated on the deposition of a homogeneous Ni–P coat containing more than 11 wt. % and studying the effect of the post-deposition heat treatment at 400 °C on microstructure development and phase transformation. It has systematically correlated between coating composition, microstructure and functional performance through a combination of SEM, EDS and XRD characterizations as well as determination of surface hardness, thermal expansion behavior, dry-sliding tribological response and resistance against corrosion in chloride environments. Through coupling these complementary analyses, the mechanism regarding performance improvement in high-phosphorus coated gray cast iron Ni–P coatings will be revealed, and the potential of such surface modification technique for improving durability and safety service life of components working under severe mechanical as well as thermal conditions will also be demonstrated.

2. Materials and Methods

2.1. Preparation of Substrate and Coating Deposition

Grey cast iron substrates were pretreated with a multistep cleaning and activation sequence to improve the coating adhesion and homogeneity. At first, the specimens were mechanically cleaned with distilled water and laboratory soap to remove loosely attached impurities and then decreased in acetone solution to ensure efficient removal of organic residue and residual surface oils. With the purpose of eliminating native oxide layers, corrosion byproducts and inclusions of rust, prior Chemical Etching is made for further purification of the surface by boiling in distilled water for 15 min. % HCl solution. After each cleaning step, samples were thoroughly rinsed with deionized water to avoid inter-step contaminations and maintain surface reactivity. The substrates were sensitized with immersion in a preheated $PdCl_2$ solution at 55°C for a few seconds before electroless deposition. Because the cast iron itself is inherently catalytic, addition of Pd-based activation resulted in an instantaneous nucleation and uniform initiation of Ni–P autocatalytic process, leading to improved coating adhesion as well as deposition kinetics [28,29].

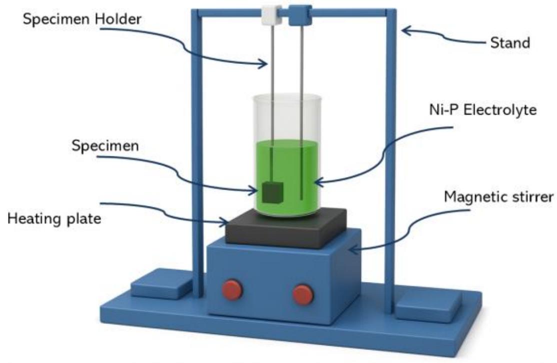

Figure 1. Electroless coating deposition process.

2.1.1. Electroless Coating Bath Composition

The plating bath as mixed according to the composition and conditions set forth in Table 1. Deposition took place in a 150ml beaker at 90±1 °C for 80 minutes. The solution pH was maintained at 5 and agitated using a magnetic stirrer (200rpm) to maintain bath uniformity. Figure (1) The deposition of the electroless coating. All reagents were weighed and mixed according to Table 1 in the order given using a class A high-precision analytical balance (model AFCOSETER 182-A, readability:0.01mg) to provide consistency for all coated samples. After the deposition, the coated samples were thermally treated at 400 °C for one hour in a vacuum for improving coating crystalline structure and adhesion. After annealing, the furnace was naturally cooled with the samples in it to prevent thermal shock and maintain the structural integrity of film.

Table 1. Bath composition of 150 mL and operating conditions of the baths utilized[30].

Nickel sulfate (g/L)	Sodium hypophosphite (g/L)	Lactic acid 88% (ml/L)	Thiourea (mg/L)	Temperature (°C)	PH
30	25	20	2	90 ± 1	5

2.2. Dry Sliding Wear Test

Both uncoated and Ni–P coated gray cast iron (GCI) samples have been produced with dimensions of 10 × 10 × 8 mm. Prior to testing, only the uncoated samples were ground utilizing SiC abrasive papers of 180, 400, 1200, and 2000 grit. All samples were stored with silica gel to ensure dryness. A pin-on-disc tribometer has beenused to assess the dry sliding wear features, as demonstrated in Figure (2). The disc-shaped specimen was assessed against a rotating steel pin at a radial distance of 2.0 mm, with a constant speed of 250 rpm under applied loads of 4 N and 8 N. The tests were performed by ASTM G99-04 [31].

2.3. Testing equipment.

Phase analysis is performed utilizing an XRD generator with a Cu target at a max tube voltage of 60 kV and a max tube current of 80 mA, with a scanning speed of 3° of 2θ per minute from 20º to 90º. Cu Kα radiation (λ = 1.5405 Å) is utilized for the XRD analysis. XRD analysis is performed utilizing the XRD-6000 Model, Shimadzu X-ray Diffractometer. The surface morphology of specimens is evaluated utilizing a scanning electron microscope (SEM). Microhardness measurements were performed utilizing a Digital Microhardness Tester HV-1000, equipped with a Vickers indenter. A load of 100 g was applied for a dwell time of 10 seconds. Measurements were taken at five various points under identical conditions, and the average magnitude was reported as the final Microhardness result. The Tafel potentiodynamic polarization behavior of both uncoated and Ni–P coated gray cast iron (GCI) samples was evaluated utilizing a DY-2323 Bi-Potentiate electrochemical workstation in a 3.5 wt.% NaCl solution. The scan rate was maintained at 1 mV/s. Electrochemical measurements were conducted in a conventional three-electrode cell configuration, where the GCI samples (with an exposed surface area of 1.0 cm²) served as the working electrode, an Ag/AgCl reference electrode was utilized during the electrochemical tests, and a platinum electrode functioned as the counter electrode.

2.4. Electrochemical Impedance Spectroscopy (EIS)

EIS measurements were performed in accordance with the widely used electrochemical testing standards; ASTM G106-89 [32] for impedance measurement and data interpretation in evaluation of corrosion performance of coatings. EIS measurements were carried out with the help of a Vertex One Potentiostat/Galvanostat/EIS equipment (Ivium Technologies, The Netherlands) connected to a personal computer for data collection and manipulation. Before impedance measurement, the working electrode was dipped in the test electrolyte until a stable OCP was obtained. EIS spectra were collected at the equilibrium OCP to reach a steady state of the interfacial conditions. A sinusoidal AC pulse was superimposed (10 mV, rms) to keep linearity of system response and to prevent disturbance on the electrochemical interface.

Impedance measurements were conducted in a frequency range of frequencies between 100 kHz and 0.1 Hz, allowing characterization of both high-frequency processes associated with the solution resistance and coating response and low-frequency processes attributed to charge-transfer resistance and diffusion-controlled corrosion mechanisms. The configuration of the electrochemical cell was adopted as a conventional three electrode system; namely, the tested specimen with or without coating acting as working electrode, and an auxiliary platinum counter electrode, whereas saturated calomel Gel reference electrode (SCE) was used.

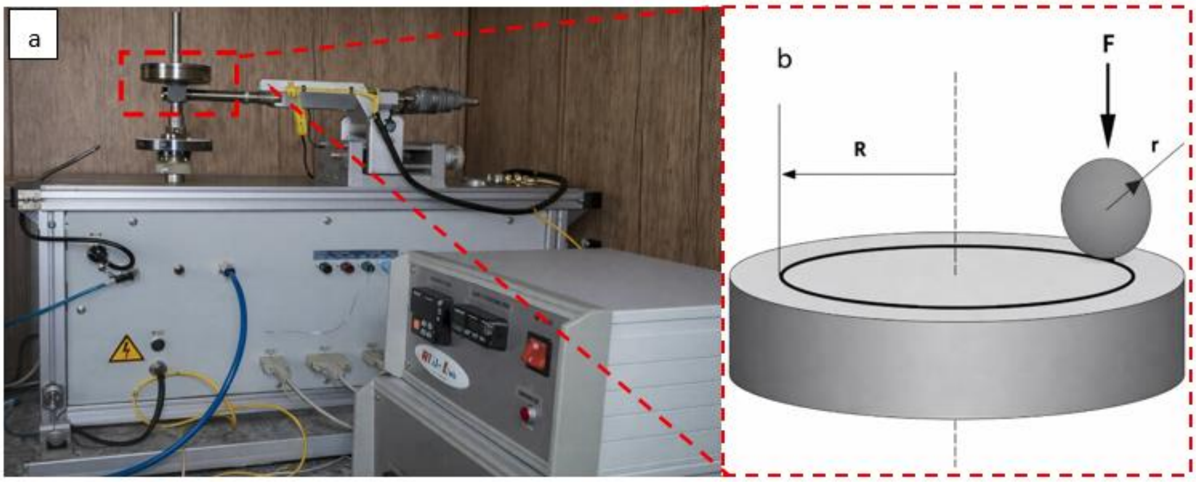

Figure 2. Schematic diagram of (a) wear test machine (TRIBOMETER model MT/60/H), (b) sample configuration of wear test.

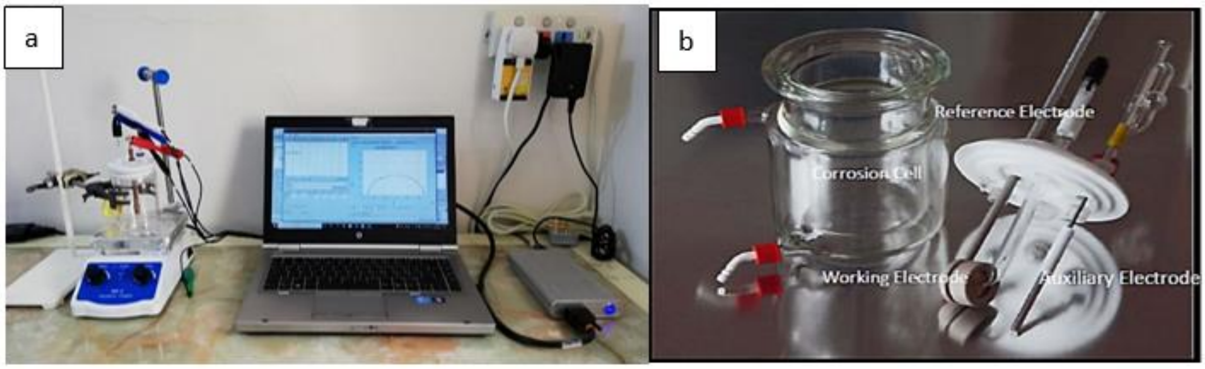

Figure 3. a)The system of corrosion/EIS measurement; b)Set up the corrosion cell and three electrodes.

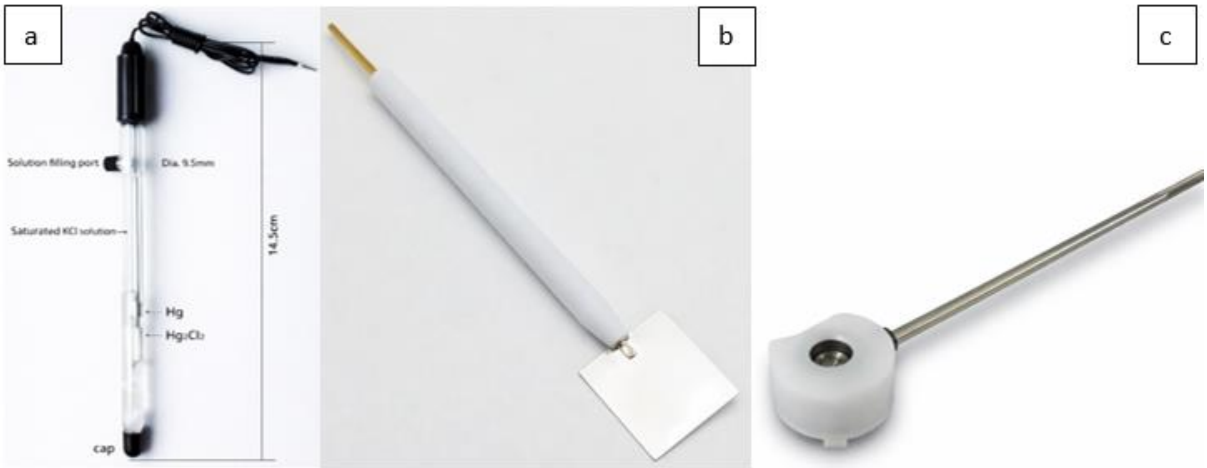

Figure 4. a) Saturated Calomel electrode; b) Platinum electrode; c) Specimen holder

3. Result and discussion

3.1. Characterization of the Ni-P Coated Surface

3.1.1. Energy Dispersive X-ray Spectroscopy(EDX)

The elemental composition of the cast iron sample surface after electroless Ni-P coating was determined utilizing Energy Dispersive X-ray Spectroscopy (EDX).The quantitative findings are presented in Table2.

Table 2. EDX analysis of the cast iron surface after electroless Ni–P coating

Element	Fe	Ni	P	Al	S	Mn	V
Weight%	73.292	14.04	11.992	0.566	0.332	0.314	0.075

The most abundant element is iron (Fe, 69.298%), suggesting that the EDX beam passed through the Ni-P layer and was applied on the cast iron substrate beneath it. They contain Ni and P with large weight percentages (14.041% and 11.992 %, respectively), which confirms the successful deposition of the Ni-P coating. This Ni–P ratio is typical of a high-phosphorous electroless deposit, which has good hardness and corrosion resistance. The contents of aluminum (Al), sulfur (S), manganese (Mn) and vanadium (V) were negligible, so that it seems that their presence does not have an important influence on coating quality. These results confirm the presence of a Ni-P layer on the surface of appropriate composition, which can enhance tribological performance after thermal treatment as indicated in [21].

3.1.2. Microhardness

Hardness is a critical parameter for evaluating the performance of protective coatings, as it directly correlates with wear resistance. Table 3 presents the microhardness findings for both the GCI substrate and the electroless Ni–P coating. The data demonstrate a significant increase in hardness from 290 HV for the uncoated substrate to 961 HV for the coated sample, reflecting an improvement of approximately 231%. This substantial enhancement is primarily because of the formation of a dense, amorphous Ni–P layer deposited in a layer-by-layer manner during the electroless plating process. Upon thermal treatment at 400 degrees centigrade, the coating undergoes partial crystallization, leading to the precipitation of Ni_3P nanocrystalline phases, which are known for their exceptional hardness. However, the measured hardness suggests that the crystallization process is not yet fully complete. Overall, these findings highlight the effectiveness of the Ni–P coating in significantly improving both the wear resistance and corrosion resistance of gray cast iron substrates, demonstrating its suitability for advanced surface engineering applications.

Hardness is an important characteristic when evaluating the performance of protective films, because it is closely related to wear resistance. The microhardness results are listed in Table 3 for the GCI substrate and for the electroless

Ni–P coating. The data show that the hardness has remarkably enhanced, increasing approximately by 3.5 times between uncoated- (290 HV) and coated- (961 HV) samples with TiO2/Ag being deposited. This significant improvement is mainly attributed to a densified, amorphous Ni–P layer generated in a layer-by-layer process of electroless plating. Upon heating at 400°C, the coating goes through a partial crystallization and nano-crystallites of superhard Ni_3P phase. The measured hardness, however, indicates anincomplete crystallization process. In general, these results emphasize that the Ni–P coating was able to remarkably enhance the wear resistance and corrosion resistance of gray cast iron substrate thereby showing its potential for advanced surface engineering application.

Table 3. MicroHardness of Substrate (GCI) and Coated (GCI/Ni-P).

	Substrate(GCI)	Coated (GCI/Ni-P)
Micro Hrdness(HV)	290	961

3.1.3. Microstructure Analysis.

The sample is graphite, as shown in the figure 3 (A and B), with randomly oriented flat lamellar flakes, typical of GCI. These flakes are due to the precipitation in solidification originating from a pearlite-rich matrix, which indicates medium carbon content and controlled cooling. It is seen that the uniform ferritic matrix is relatively soft while the pearlitic structure, which consists of alternating layers made up of ferrite and cementite provides with higher hardness and wear resistance [33].The measured microhardness of the sample is 290 HV, in agreement with literature values usually found for pearlitic gray cast iron, typically varying from 250 to 320 HV [34]. Figure 3-C, D and E shows the SEM image of GCI surface morphology after electroless Ni-P coating. The surface of the electroless Ni–P coating appears non-uniformly distributed, and it is randomly covered with small nodule features and irregular texturing. This appearance is a characteristic of the high-phosphorus content (11.04 wt.%) Ni–P coatings. %, which favors the formation of nanocrystalline or amorphous phase. The formed microcracks and pores are attributed to the hydrogen evolution during the entire immersion plating process, or a residue stress occurring due to the difference of thermal expansion coefficient between Ni–P coatings and GCI substrates. Notwithstanding the surface defects, the coating shows an equally spread and well adhered coated region (good interface adhesion) with a uniform protection on the substrate, suggesting that its deposition process is efficient for creating a continuous and protective barrier.

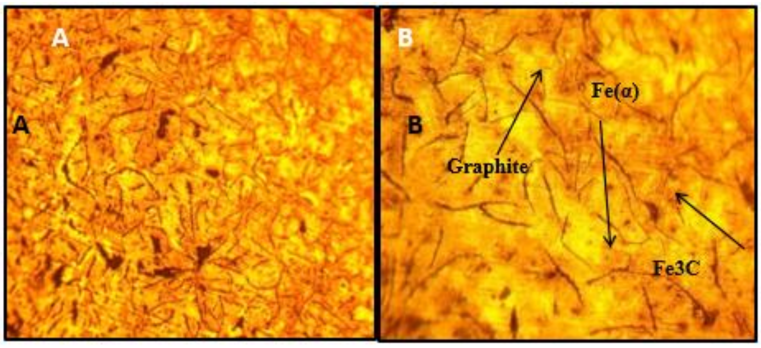

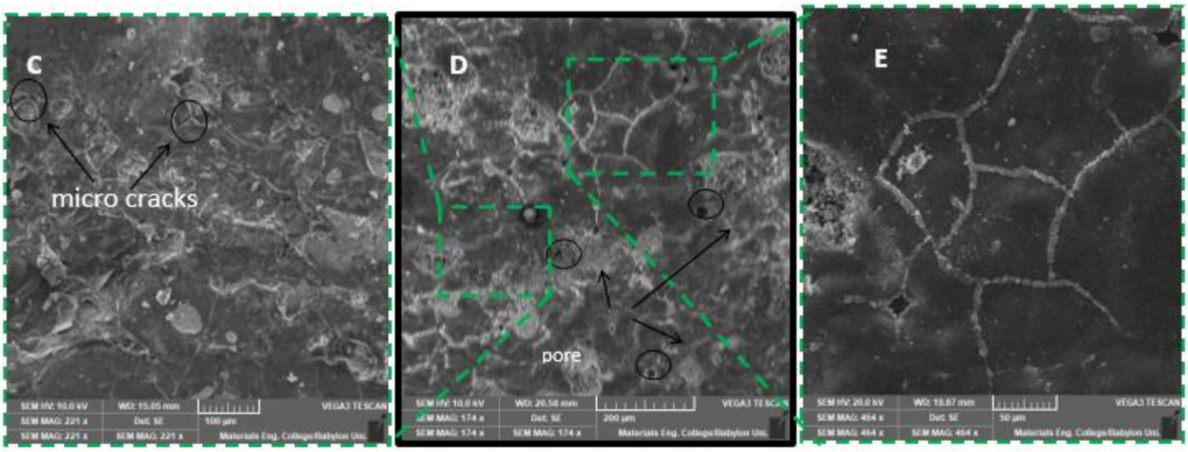

Figure 5. (A, B) Microstructure of GCI substrate at 200X and 600X, respectively ; (C, D, E) Electroless Ni–P coated GCI demonstrating surface morphology and coating characteristics.

3.1.4. X-Ray Diffraction Analysis of Ni-P Coating

The XRD patterns of both uncoated and Ni-P-coated gray cast iron (GCI) are demonstrated in Figure 4 . The uncoated GCI sample exhibits sharp diffraction peaks corresponding to α-Fe and Fe_3C, which aligns with the pearlitic structure commonly found in gray cast iron. After coating with electroless Ni–P and thermal treatment at 400 degrees centigrade, the XRD pattern of the coated sample demonstrates noticeable changes. Although the α-Fe peaks remain visible, the X-ray penetrating through the coating to the substratenew diffraction peaks appear at approximately $2\theta \approx 40°$, 45°, and 48°, which correspond to the (111), (201), and (210) planes of the Ni_3P phase, indicating that partial crystallization has occurred within the coating. The formation of Ni_3P is affected by the phosphorus amount controlled by the sodium hypophosphite amount in the plating bath as well as the deposition and thermal treatment conditions.

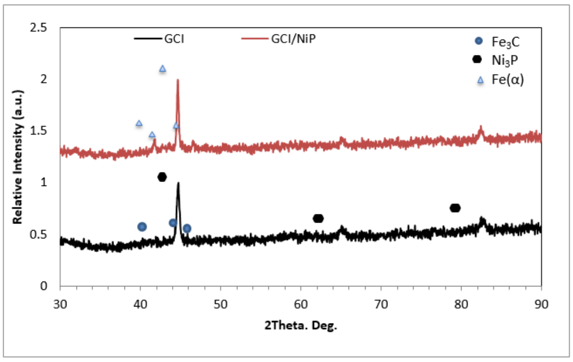

Figure 6. The XRD patterns of GCI and electroless Ni–P coating.

The existence of Ni_3P contributes to the increased hardness of the coating and suggests improved chemical and mechanical stability. Additionally, the broader and less intense peaks in the coated sample indicate a fine-grained or partially amorphous structure, which is typical for high-phosphorus Ni–P coatings[35].

High-phosphorus electroless Ni–P coatings (>10 wt.% P) are thermodynamically predisposed to retain amorphous structure due to suppressed long-range atomic diffusion and increased activation energy for crystallization, even after annealing at moderate temperatures (400 °C) [36,37]. Previous studies have reported that, under similar heat treatment conditions, partial crystallization with predominant nanocrystalline Ni_3P formation is more probable than complete transformation [38,39]. The functional co-existence of amorphous and nanocrystalline phases has also been linked to enhanced corrosion resistance and tribological performance [40,41]. XRD patterns of as-deposited coatings typically exhibit a broad halo characteristic of amorphous phases, with the emergence of Ni_3P diffraction peaks only after heat treatment, thereby justifying inclusion of both patterns in the present study [42,43].

3.2. Coefficient of Thermal Expansion (CTE) Analysis

Figure (5) shows the CTE-temperature curves of two GCI samples, the substrate without coating, and the Ni–P coated specimen. Both show a usual linear CTE-temperature behaviour. However, exception can be made for the measurements above 200°C, where the uncoated CTE is larger than that of a coated one (i.e., $0.25\times10^{-6}C^{o-1}$ against $0.19\times10^{-6}C^{o-1}$). This reduction is associated with the dense, uniform and amorphous or nano-crystalline structure of Ni–P coating as supported from SEM Figure 3-D which lends itself better dimensional stability under thermal loading. The results describe a promising prospect for the Ni–P coatings in application requiring high temperature, where thermal stability, wear resistance and surface durability are of importance, such as engine parts, molds and heat exchange surfaces. The SEM measurement conducted post-thermal expansion test in Figure 6 does not indicate any crack, delamination or spallation in the Ni–P coating layer; consequently, its excellent adhesion and thermal stability was verified [44].

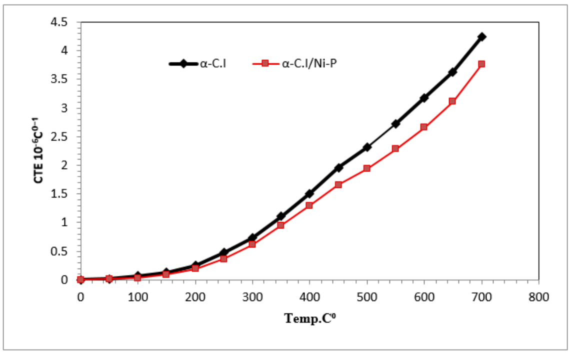

Figure 7. The CTE versus temperature for two GCI samples, the uncoated substrate, and the Ni–P coated specimen.

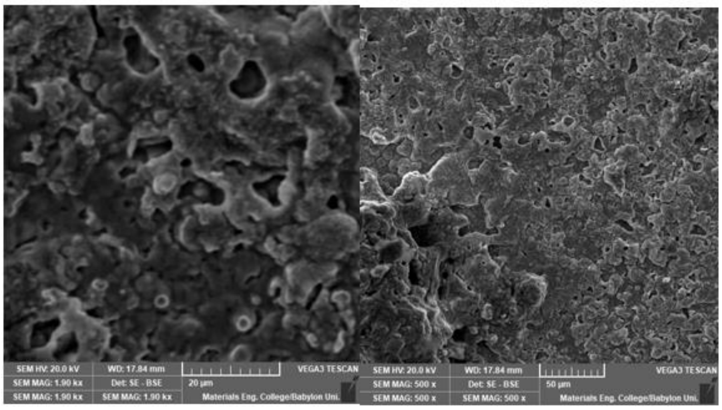

Figure 8. Ni-P coated after the thermal expansion test.

3.3. Electrochemical Behavior Of Ni-P Coated Cast Iron

The potentiodynamic polarization curves of both untreated and electroless Ni–P coated GCI substrate in 3.5% NaCl solution are shown in Fig. The corrosion resistance of the samples was assessed by Tafel analysis. The Ecorr value of the Ni–P coated electrode (+0.484 V) was more positive than that for uncoated substrate (Ecorr = –0.625 V), indicating an improved resistance to corrosion initiation. Moreover, the Rp of the coated sample was around (4.96 Ω. cm2), much greater than the uncoated sample (4.03 Ω. cm2), indicating improved barrier properties. However, the uniform appearance of surface following electroless Ni–P deposition (since Ni–P deposit itself serves as well protected layer) proved to be highly resistant against corrosion due to the formation of protective scale over the cast iron which retard charge transfer and inhibit anodic dissolution Better corrosion resistance performance associated with a high chemical resistivity was synthesized by changing amorphous structure in case of orthorhombicC6and do not form passivation films. The absence of dislocations, grain boundaries and other structural defects in the coating plays a major role in enhancing corrosion resistance. This homogeneity in the structure contributes to the formation of a stable passivation film that provides protection from corrosive media. Comparative work [22]of nanocrystalline, amorphous, and annealed nanocrystalline Ni–P alloys proves that the amorphous state in Ni–P alloy is more resistant to corrosion owing to its homogeneous microstructure and no preferred corrosion paths.

Table 4. Electrochemical Parameters from Tafel Analysis.

Samples	E_{corr} (V)	I_{corr} (A/cm²)	ba (mV/dec)	bc (mV/dec)	Rp ($\Omega.cm^2$)
Un coated	–0.625	2.088×10^{-4}	9.709	2.425	4.03
Coated Ni-P	–0.484	2.239×10^{-4}	7.906	3.777	4.96

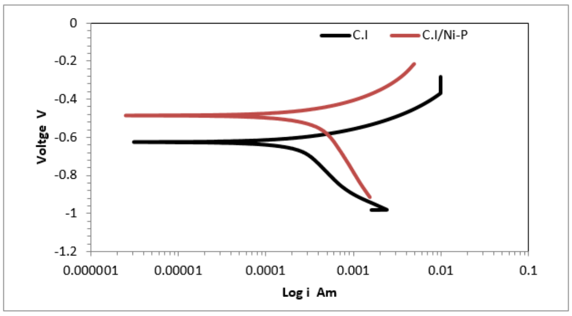

Figure 9. Polarization curves of uncoated and electroless Ni–P coated cast iron.

3.4. Tribological behavior of Ni-P coated cast Iron.

Figures (8) and (9) present the wear behavior of cast iron with or without electroless Ni–P coating under applied loads of 4 N and 8 N, before and after such a coating.The reports provide the error in data-points. Before the application of an Electroless Ni– P, The uncoated specimens exhibited an ever-increasing COF to stabilize from 0.55 to 0.65. Several deep drops in COF were recorded, which indicating a repetition of losing stable sliding again. 16 These oscillations are caused by severe adhesive wear, local plastic deformation, and delamination of the surface oxide film. This behavior provides powerful evidence to demonstrate the poor wear resistance of naked cast iron, especially under high-load state. It indicates the weak tribo-film can be generated and worn away continuously since of its low surface strength.

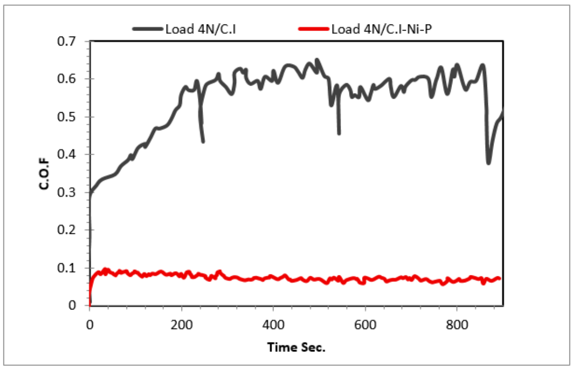

Figure 10. The COF againstTime for two GCI samples, the uncoated substrate, and the Ni–P coated sampleunder an applied load of 4 N.

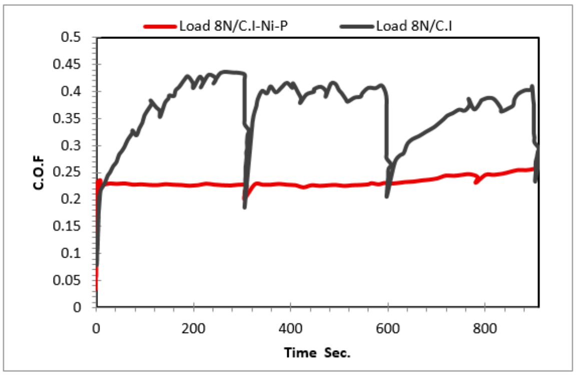

Figure 11. The COF against Time for two GCI samples, the uncoated substrate, and the Ni–P coated sample under an applied load of 8 N.

The Ni–P coated sample exhibited much improved tribological properties, with a relatively low and stable COF of 0.07 to 0.1 during the test. The reduction of the COF is to be attributed directly to an increased surface hardness and better load-carrying capacity arising from the electroless Ni–P coating. This hard and dense coating decreases the surface deformation and prohibits adhesive interactions during sliding, therefore exhibit superior tribological properties [45]. The high hardness of the coating improves resistance to plastic deformation and surface failure, which yields more stable and uniform friction behaviors, this is in line with SEM analysis of the wear-tracks. Surface morphology(Figure 10) examination of the surface-coated sample reveal smooth and low-depth wear tracks without visible cracks, peeling, spalling or coating damage; this suggest that there are sufficient Ni–P maintained as a balustrade during sliding process to reduce direct material contact and metal-wear. The SEM image of the uncoated cast iron shows tremendous surface damage with deep grooving, abrasive wear and loose fragments implying an aggressive wear mechanism which characterized by adhesion and micro cutting as shown in Figure (10-A).

3.5. Electrochemical Impedance Spectroscopy (EIS)

The electrochemical impedance spectroscopy (EIS) results (Figs. 13 and 14) clearly reveal the better corrosion protection of the electroless Ni–P coating on grey cast iron in 3.5 wt.% NaCl solution compared to that of both bare substrate and modified sample. The Nyquist plot of the coated sample shows a much more elongated and depressed capacitive loop with respect to the bare substrate, confirming that interface impedance significantly increases demonstrating an enhanced improvement in charge transfer resistance. Quantitatively, the polarization resistance of Ni–P coated sample (Rp = 2094 Ω) is obviously higher than that of uncoated cast iron (Rp = 1593 Ω), indicating that the coating successfully retards the electrochemical activity at the metal–electrolyte interface. This behavior is typical for a dense electroless Ni–P coating that functions as both physical and anodic barriers to ionic transport, with less effective active area exposed to corrosive environment. The equivalent circuit fitting also implicates two separate electrochemical time constants for the coating layer and substrate interface, which have been frequently described as being related with nickel-based corrosion protective coatings in chloride containing media. Significantly, however maximum impedance is also significantly higher than the natural PZT, which can be attributed to the presence of micro-porosity inherent in electroless depositions that adds a gradualness component and longer diffusional path for corrosion propagation. These results are in good agreement with recent works that found the Nyquist semicircle diameters, polarization resistance and long-term electrochemical stability of electroless Ni–P coatings on ferrous substrates are greater in saline solutions than unstabilized materials [46–49].

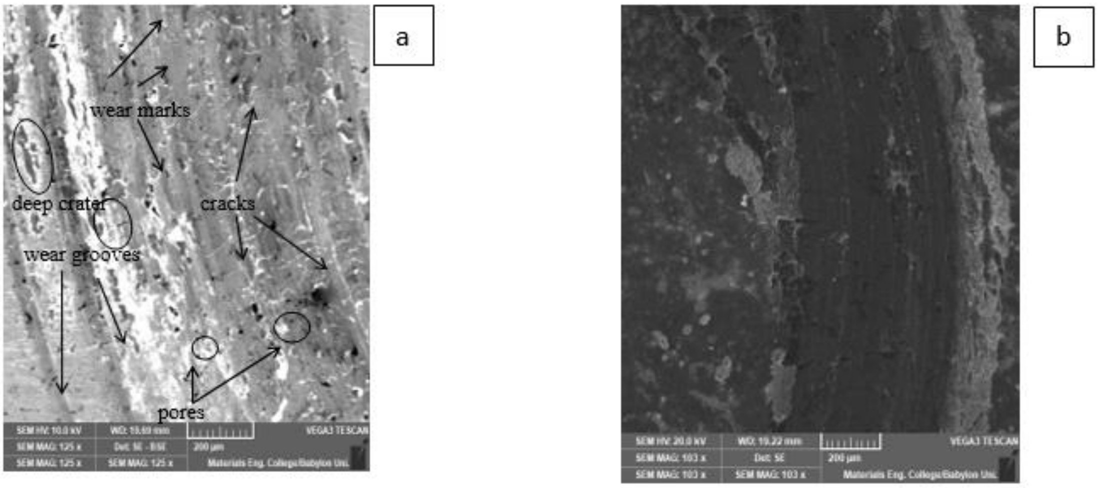

Figure 12. SEM images of the wear tracks on GCI samples: a) uncoated;b)Ni–P coated samples.

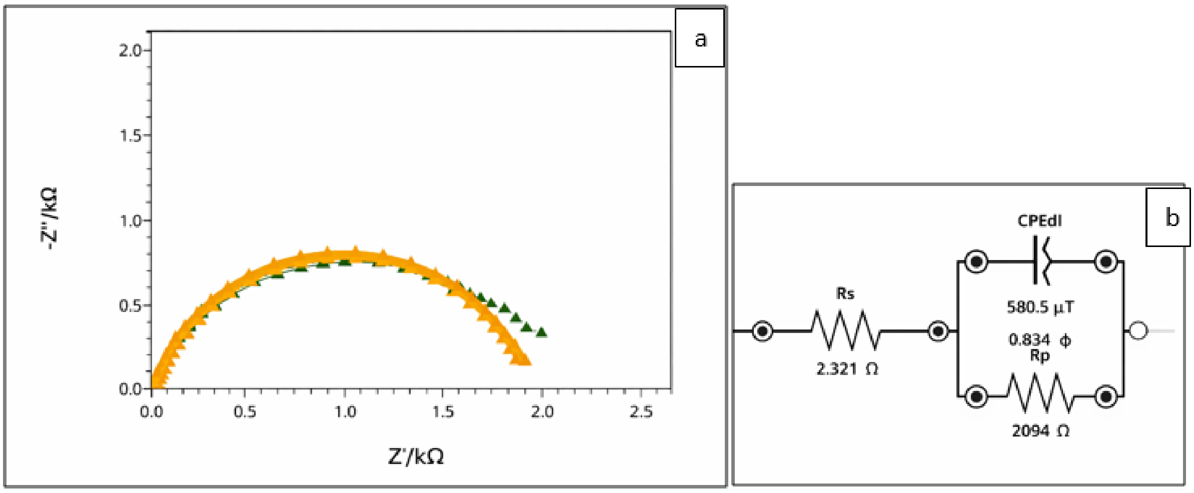

Figure 13. a) Impedance plots of grey cast iron with coatingof immersion in a 3.5% NaCl solution;b) Equivalent circuit for grey cast iron with coating.

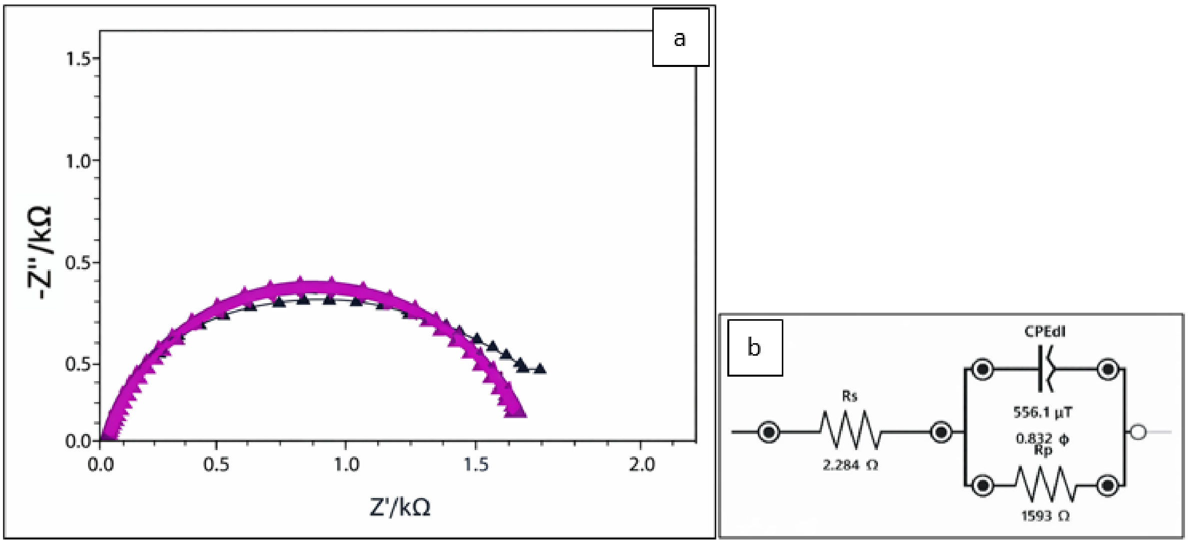

Figure 14. a) Impedance plots of grey cast iron without coatingofimmersion in a 3.5% NaCl solution; b) equivalent circuit for grey cast iron with coating.

4. Conclusion

This study systematically demonstrates the effectiveness of electroless high-phosphorus Ni–P coatings in enhancing the mechanical, thermal, tribological, and electrochemical performance of gray cast iron (GCI). Microstructural and compositional analyses confirmed the successful deposition of a uniform Ni–P coating with a phosphorus content of approximately 12 wt.%, classifying the coating as a high-phosphorus system. Post-deposition heat treatment at 400 °C induced partial crystallization, evidenced by the formation of nanocrystalline Ni_3P phases embedded within a predominantly amorphous matrix, which provided a favorable balance between hardness, structural stability, and corrosion resistance.

The Ni–P coating led to a substantial improvement in surface mechanical properties, increasing the microhardness from 290 HV for the uncoated substrate to 961 HV for the coated specimen. Thermal expansion measurements revealed enhanced dimensional stability of the coated GCI, with the coefficient of thermal expansion reduced from 0.25×10^{-6} to 0.19×10^{-6} °C^{-1}, highlighting the coating's suitability for applications involving thermal fluctuations. Electrochemical investigations in 3.5 wt.% NaCl solution showed a positive shift in corrosion potential and an increase in polarization resistance, indicating improved resistance to corrosion initiation and propagation. Electrochemical impedance spectroscopy further confirmed superior barrier performance of the Ni–P coating, as reflected by the enlarged Nyquist capacitive loop and higher polarization resistance relative to the uncoated GCI.

Tribological evaluation under dry sliding conditions revealed a marked reduction in the coefficient of friction from approximately 0.65 for the uncoated substrate to 0.07–0.10 for the Ni–P coated samples, accompanied by significantly reduced wear damage and preserved coating integrity. SEM observations of the wear tracks corroborated the transition from severe adhesive–abrasive wear in the uncoated GCI to mild and stable sliding behavior in the coated system, attributable to the high hardness and load-bearing capacity of the Ni–P layer.

References

[1] O. Azouani, M. Keddam, O. Allaoui, A. Sehisseh, "Kinetics of the formation of boride layers on EN-GJL-250 gray cast iron", Materials Performance and Characterization, Vol. 6, 2017, pp. 510-522.https://doi.org/10.1520/MPC20160077

[2] B. Singh, J.S. Grewal, R. Kumar, S. Sharma, A. Kumar, K.A. Mohammed et al., "Novel study on investigating the mechanical, microstructure morphological, and dry sliding wear characteristics of grey cast iron GG25 with copper additions for valve guides in internal combustion engine", Frontiers in Materials, Vol. 10, 2024, Article 1293254.https://doi.org/10.3389/fmats.2023.1293254

[3] Laouissi, M.A. Yallese, A. Belbah, A. Khellaf, A. Haddad, "Comparative study of the performance of coated and uncoated silicon nitride (Si_3N_4) ceramics when machining EN-GJL-250 cast iron using the RSM method and 2D and 3D roughness functional parameters", Journal of the Brazilian Society of Mechanical Sciences and Engineering, Vol. 41, 2019. https://doi.org/10.1007/s40430-019-1708-9

[4] Hammood, H. Mahdi, "Development of an artificial neural network model to study the influence of oxidation process and zinc electroplating on fatigue life of gray cast iron", International Journal of Mechanical and Mechatronics Engineering, Vol. 12, 2012, pp. 128-136.

[5] ASM International, Properties and Selection: Irons, Steels, and High-Performance Alloys, ASM Handbook, Vol. 1, 1990. https://doi.org/10.31399/asm.hb.v01.9781627081610

[6] W. Sun, A.W.-Y. Tan, D.J.Y. King, N.W. Khun, A. Bhowmik, I. Marinescu et al., "Tribological behavior of cold sprayed Inconel 718 coatings at room and elevated temperatures", Surface and Coatings Technology, Vol. 385, 2020, Article 125386. https://doi.org/10.1016/j.surfcoat.2020.125386

[7] J. Gussmagg, M. Maier, M. Pusterhofer, F. Grün, "EHD simulation study on the influence of measured ICE compression piston ring profiles on the lubrication film formation", Tribology International, Vol. 199, 2024, Article 110015. https://doi.org/10.1016/j.triboint.2024.110015

[8] N.S. Radhi, Z.S. Al-Khafaji, "Investigation of biomedical corrosion of implant alloys in physiological environment", International Journal of Mechanical and Production Engineering Research and Development, Vol. 8, 2018.https://doi.org/10.24247/ijmperdaug201827

[9] N.M. Dawood, N.S. Radhi, Z.S. Al-Khafaji, "Investigation of corrosion and wear behavior of nickel-nano silicon carbide

coating on stainless steel 316L", Materials Science Forum, Vol. 1002, 2020, pp. 33-43. https:// doi.org/10.4028/www.scientific.net/MSF.1002.33

[10] N.S. Radhi, M. Marza, Z.S. Al-Khafaji, "Modification of electroless nickel-phosphorus coatings by adding zirconia particles", Solid State Technology, Vol. 63, 2020.

[11] M. Jabor, N.S. Radhi, M.A. Al-Kinani, Z.S. Al-Khafaji, "Optimization of electroless nickel-based coating for cermet cutting tools substrate", Journal of Mechanical Engineering Research and Developments, Vol. 44, 2021, pp. 30-40.

[12] S. Sarkar, R. Mandal, N. Mondal, S. Chaudhuri, T. Mandal, G. Majumdar, "Modelling and prediction of micro-hardness of electroless Ni-P coatings using response surface methodology and fuzzy logic", Jordan Journal of Mechanical and Industrial Engineering, Vol. 16, 2022.

[13] Atulkar, R.K. Pandey, P.M.V. Subbarao, "Role of textured piston rings/liners in improving the performance behaviours of IC engines: A review with vital findings", Surface Topography: Metrology and Properties, Vol. 9, 2021, Article 023002. https://doi.org/10.1088/2051-672X/ac0a36

[14] T. Suthisripok, P. Semsamran, "The impact of biodiesel B100 on a small agricultural diesel engine", Tribology International, Vol. 128, 2018, pp. 397-409. https://doi.org/10.1016/j.triboint.2018.07.042

[15] V. Fox, A. Jones, N.M. Renevier, D.G. Teer, "Hard lubricating coatings for cutting and forming tools and mechanical components", Surface and Coatings Technology, Vol. 125, 2000, pp. 347-353. https:// doi.org/10.1016/S0257-8972(99)00611-8

[16] C.A. Loto, "Electroless nickel plating - A review", Silicon, Vol. 8, 2016, pp. 177-186. https:// doi.org/10.1007/s12633-015-9367-7

[17] ASTM B733-22, Standard Specification for Autocatalytic (Electroless) Nickel-Phosphorus Coatings, ASTM International, West Conshohocken, PA, USA, 2022. https:// doi.org/10.1520/B0733-22

[18] M. Buchtík, P. Kosár, J. Wasserbauer, J. Tkacz, P. Doležal, "Characterization of electroless Ni-P coating prepared on a wrought ZE10 magnesium alloy", Coatings, Vol. 8, 2018, Article 96. https://doi.org/10.3390/coatings8030096

[19] G. Zhao, R. Wang, S. Liu, D. Wu, Y. Zhang, T. Wang et al., "Role of molybdenum in improving thermal stability and corrosion resistance of amorphous Ni-P deposits", Journal of Non-Crystalline Solids, Vol. 549, 2020, Article 120358. https://doi.org/10.1016/j.jnoncrysol.2020.120358

[20] S. Sarkar, A. Mukherjee, R.K. Baranwal, J. De, C. Biswas, G. Majumdar, "Prediction and parametric optimization of surface roughness of electroless Ni-Co-P coating using Box-Behnken design", Journal of Mechanical Behavior of Materials, Vol. 28, 2019, pp. 153-161. https://doi.org/10.1515/jmbm-2019-0017

[21] D.R. Dhakal, Y.U. Han, B.G. Lee, T.H. Kim, G.B. Jang, S.Y. Cho, "Wear resistance behavior of low-, mid-, and high-phosphorus electroless Ni-P coatings heat-treated in air", Coatings, Vol. 14, 2024, Article 648. https://doi.org/10.3390/coatings14050648

[22] Z. Li, M. Luo, H. Mao, C. Bian, "Crystallization and electrochemical corrosion behaviors of nanometer amorphous Ni-P alloys", Materials Research Express, Vol. 7, 2020, Article 026418. https://doi.org/10.1088/2053-1591/ab769f

[23] Balegh, H. Trouzine, Y. Houmadi, "Finite element simulation and prediction of mechanical and electrochemical behavior of crevice corrosion in sheet pile steel", Jordan Journal of Mechanical and Industrial Engineering, Vol. 12, 2018.

[24] Lelevic, "Ni-P coatings electroplating - A review, Part I: Pure Ni-P alloy", arXiv Preprint, arXiv:1807.04693, 2018.

[25] S. Wang, C. Ma, F.C. Walsh, "Alternative tribological coatings to electrodeposited hard chromium", 2020, pp. 1-35.

[26] J.C. Avelar-Batista, E. Spain, M. Letch, J. Housden, R. Beechey, "Improvements in wear resistance of high thermal conductivity copper alloys using electroless Ni-P coating prior to PVD deposition", Surface and Coatings Technology, Vol. 201, 2006, pp. 4052-4057.https://doi.org/10.1016/j.surfcoat.2006.08.038

[27] U.S. Waware, A.M.S. Hamouda, N.P. Wasekar, "Mechanical properties, thermal stability, and corrosion behavior of electrodeposited Ni-B/AIN nanocomposite coating", Surface and Coatings Technology, Vol. 337, 2018, pp. 335-341.https://doi.org/10.1016/j.surfcoat.2018.01.028

[28] Ahmadi Ashtiani, S. Faraji, S.A. Iranagh, A.H. Faraji, "Electroless Ni-P alloys with different complexing agents on CK45 steel substrate", Arabian Journal of Chemistry, Vol. 10, 2017, pp. S1541-S1545. https://doi.org/10.1016/j.arabjc.2013.05.015

[29] H. Zhang, J. Zou, N. Lin, B. Tang, "Review on electroless Ni-P coatings for improving surface performance of steel", Surface Review and Letters, Vol. 21, 2014, Article 1430002. https://doi.org/10.1142/S0218625X14300020

[30] Ashtiani A.A., Faraji S., Iranagh S.A., Faraji A.H., "The study of electroless Ni-P alloys with different complexing agents on CK45 steel substrate", Arabian Journal of Chemistry, Vol. 10, 2017, pp. S1541-S1545.https://doi.org/10.1016/j.arabjc.2013.05.015

[31] ASTM G99-04, Standard Test Method for Wear Testing with a Pin-on-Disk Apparatus, ASTM International, 2004.

[32] ASTM G106-15, Standard Practice for Verification of Algorithm and Equipment for Electrochemical Impedance Measurements, ASTM International, West Conshohocken, PA, USA, 2015.

[33] J.A.G. de Sousa, W.F. Sales, A.R. Machado, "A review on the machining of cast irons", *International Journal of Advanced Manufacturing Technology*, Vol. 94, 2017, pp. 4073–4092. https://doi.org/10.1007/s00170-017-1140-1

[34] M.M. Jabbari Behnam, P. Davami, N. Varahram, "Effect of cooling rate on microstructure and mechanical properties of gray cast iron", *Materials Science and Engineering A*, Vol. 528, 2010, pp. 583–588. https://doi.org/10.1016/j.msea.2010.09.087

[35] A.M. Pillai, A. Rajendra, A.K. Sharma, "Electrodeposited nickel–phosphorous alloy coating: preparation, properties, and structural transitions", *Journal of Coatings Technology and Research*, Vol. 9, 2012, pp. 785–797. https://doi.org/10.1007/s11998-012-9411-0

[36] J.D. Lin, C.T. Chou, "Influence of phosphorus content on microstructure and specific capacitance of etched electroless Ni-P coatings", *Surface and Coatings Technology*, Vol. 368, 2019, pp. 126–137. https://doi.org/10.1016/j.surfcoat.2019.04.009

[37] M. Tian, Z. Jian, R. Hai, F. Chang, "Non-isothermal crystallization kinetics of amorphous electroless Ni-P alloy plating", *Journal of Thermal Analysis and Calorimetry*, Vol. 148, 2023, pp. 1959–1970.https://doi.org/10.1007/s10973-022-11828-0

[38] M. Buchtík, L. Doskočil, R. Brescher, P. Doležal, J. Másilko, J. Wasserbauer, "Effect of crystallization and phase transformation on mechanical and electrochemical corrosion properties of Ni-P coatings", *Coatings*, Vol. 11, 2021, Article 447.https://doi.org/10.3390/coatings11040447

[39] J. Wojewoda-Budka, A. Wierzbicka-Miernik, L. Lityńska-Dobrzyńska, M.J. Szczerba, G. Mordarski, M. Mosiałek et al., "Microstructure and phase transformations of Ni-P and Ni-P-Re electroless coatings after heat treatment", *Electrochimica Acta*, Vol. 209, 2016, pp. 183–191. https://doi.org/10.1016/j.electacta.2016.05.043

[40] M. Lou, K. Xu, L. Chen, C. Hong, Y. Yuan, Y. Du et al., "Development of robust surfaces for harsh service environments from the perspective of phase formation and transformation", *Journal of Materials Informatics*, Vol. 1, 2021.https://doi.org/10.20517/jmi.2021.02

[41] J. Ding, W. Zhuang, Q. Wang, H. Mei, D. Zhao et al., "Tailoring the microstructure and properties of HiPIMS-

deposited DLC-Cr nanocomposite films via chromium doping", *Nanomaterials*, Vol. 16, 2026, Article 150.https://doi.org/10.3390/nano16020150

[42] Sadeghi, *Microstructure Evolution and Strengthening Mechanisms in Ni-Based Composite Coatings*, PhD Thesis, 2016.

[43] L. Ma, "Electrochemical and morphological characterization of electroless Ni-P coatings on diamond particles", 2020.

[44] Ahmadkhaniha, F. Eriksson, C. Zanella, "Optimizing heat treatment for electroplated Ni-P and Ni-P/SiC coatings", *Coatings*, Vol. 10, 2020, Article 1179. https://doi.org/10.3390/coatings10121179

[45] S. Kumar, T. Banerjee, D. Patel, "Tribological characteristics of electroless multilayer coatings: A review", *Materials Today: Proceedings*, Vol. 33, 2020, pp. 5678–5682.https://doi.org/10.1016/j.matpr.2020.04.207

[46] Y. Zhang, N.S. Mbugua, H. Jin, L. Chen, "Preparation and investigation of Ni-Co-P alloy coatings using jet electrodeposition with varying pulse parameters", *Crystals*, Vol. 13, 2023, Article 303.https://doi.org/10.3390/cryst13020303

[47] N. Ortiz, J.R. González-Parra, J. Olaya, D. Agredo, R. Valdez, H. Waage et al., "Morphological and corrosion characterization of electroless Ni-P coatings deposited on ductile iron", *Coatings*, Vol. 14, 2024.https://doi.org/10.3390/coatings14101317

[48] Y. Meng, Y. Zhao, J. Zhong, Y. Liao, D. Chen, "Effect of plating time on surface morphology and corrosion behavior of electroless Ni-P coating in simulated concrete pore solution", *Case Studies in Construction Materials*, Vol. 21, 2024, Article e03497.

[49] S.Y. Ahmed, S.B. Mahmoud, M.A. Shoeib, "Synthesis, structure characterization, and corrosion properties of duplex electroless Ni-P/Ni-B and Ni-P/Ni-BW coatings on mild steel", *Scientific Reports*, Vol. 14, 2024, Article 24983.https://doi.org/10.1038/s41598-024-75883-3